# Earthquake-induced deformation analyses of the Upper San Fernando Dam under the 1971 San Fernando Earthquake

**Guoxi Wu**

**Abstract**: A nonlinear effective stress finite element approach for dynamic analysis of soil structure is described in the paper. Major features of this approach include the use of a third parameter in the two-parameter hyperbolic stress–strain model, a modified expression for unloading–reloading modulus in the Martin–Finn–Seed pore-water pressure model, and an additional pore-water pressure model based on cyclic shear stress. The additional pore-water pressure model uses the equivalent number of uniform cyclic shear stresses for the assessment of pore-water pressure. Dynamic analyses were then conducted to simulate the seismically induced soil liquefaction and ground deformation of the Upper San Fernando Dam under the 1971 San Fernando Earthquake. The analyses were conducted using the finite element computer program VERSAT. The computed zones of liquefaction and deformation are compared with the measured response and with results obtained by others.

*Key words*: effective stress method, finite element analysis, Upper San Fernando Dam, earthquake deformation, VERSAT.

**Résumé** : Dans cet article, on décrit une approche d'éléments finis en contraintes effectives non linéaires pour l'analyse dynamique de la structure du sol. Les principales caractéristiques de cette approche comprennent l'utilisation d'un troisième paramètre dans le modèle parabolique contrainte–déformation à deux paramètres, l'utilisation d'une expression modifiée pour le module de déchargement-rechargement dans le modèle de pression interstitielle de Martin–Finn–Seed, et l'utilisation d'un modèle additionnel de pression interstitielle basé sur la contrainte de cisaillement cyclique. Le modèle additionnel de pression interstitielle utilise le nombre équivalent de contraintes de cisaillement cycliques uniformes pour évaluer la pression interstitielle. On a alors réalisé des analyses dynamiques pour simuler la liquéfaction du sol induite par un séisme et la déformation du terrain du Upper San Fernando Dam au cours du tremblement de terre de San Fernando de 1971. Les analyses ont été réalisées au moyen du programme d'ordinateur d'éléments finis VERSAT. Les zones calculées de liquéfaction et de déformation ont été comparées avec la réponse mesurée et avec les résultats obtenus par d'autres.

*Mots clés* : méthode de contrainte effective, analyse en éléments finis, Upper San Fernando Dam, déformation due au tremblement de terre, VERSAT.

[Traduit par la Rédaction]

## Introduction

Assessment of earthquake-induced soil liquefaction and resulting ground deformation is a major problem in geotechnical earthquake engineering. Although the first part of the problem has been dealt with in great depth (Seed and Idriss 1970; Seed and Harder 1990; Finn 1998), the second part of the problem remains a challenging task. Quantifying earthquake-induced ground deformation is now a critical element in an earthquake-related geotechnical assignment.

Methods for earthquake-induced deformation analysis vary from some variation of Newmark's rigid-block-sliding approach (Newmark 1965) to the nonlinear effective stress analysis carried out in "a direct and fundamental manner." The Newmark type of deformation analysis is often adopted to give a very crude first-cut estimation of deformation without involving more complicated numerical analysis. The fundamental nonlinear analysis of dynamic response involves the use of elastic–plastic models of soil behavior under cyclic loading. The elastic–plastic models are generally based on a kinematic hardening theory of plasticity using either multiyield surfaces or a boundary surface theory with a hardening law giving the evolution of the plastic modulus. Saturated soil is treated as a two-phase material using Biot's coupled equations for the soil and water phases. These constitutive models are complex and incorporate some parameters not usually measured in field or laboratory testing. Typical elastic–plastic models used in current engineering practice are represented by DYNAFLOW (Prevost 1981), DYSAC2 (Muraleetharan et al. 1988), and SWANDYNE4 (Zienkiewicz et al. 1990*a*, 1990*b*). Performance of the fully coupled effective stress models has been reported from the Verification of Liquefaction Analysis by Centrifuge Studies (VELACS) Project (Popescu and Prevost 1995).

The direct nonlinear approach is based on direct modeling of soil nonlinear hysteretic stress–strain response. The direct

Received November 11, 1999. Accepted August 10, 2000. Published on the NRC Research Press Web site on December 21, 2000.

**G. Wu.** EBA Engineering Consultants Ltd., 550-1100 Melville Street, Vancouver, BC V6E 4A6, Canada.

 DOI: 10.1139/cgj-38-1-1 © 2001 NRC Canada

**Fig. 1.** Measured displacement at the Upper San Fernando Dam (modified from Serff et al. 1976).

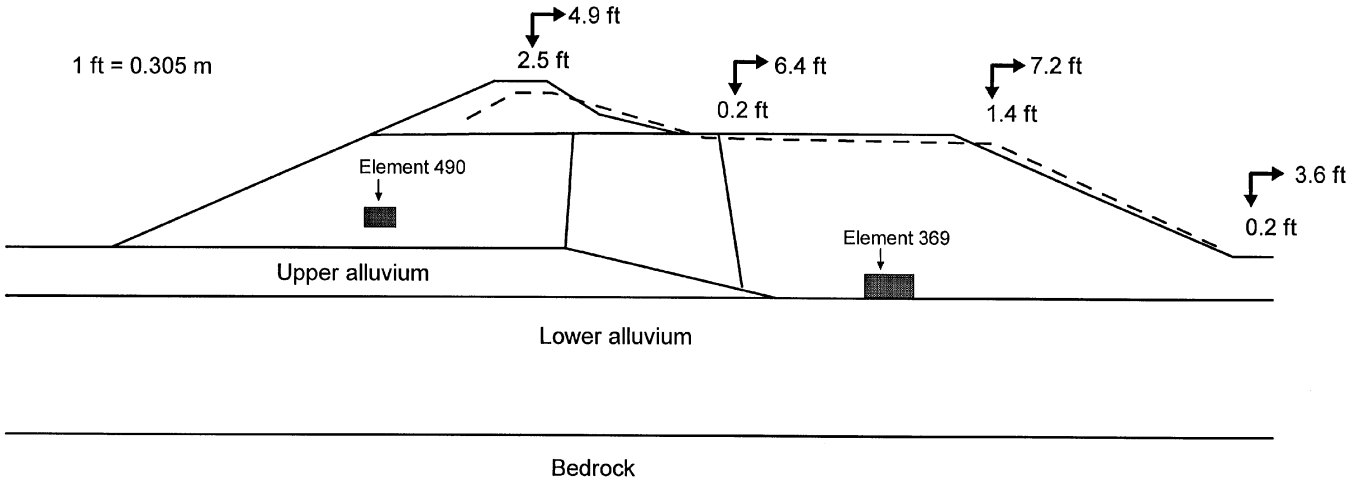


nonlinear dynamic effective stress analysis is represented by the finite element program TARA-3 (Finn et al. 1986). This direct nonlinear approach is often used in the final design of remediation schemes in seismic rehabilitation projects (Finn 1998; Finn et al. 1999). The deformation analysis of Finn et al. (1996) uses the nonlinear hyperbolic stress–strain soil model and the Martin–Finn–Seed (MFS) (Martin et al. 1975) model for pore-water pressure calculation and soil liquefaction assessment. The hyperbolic stress–strain model is simple and its parameters can be readily evaluated. On the other hand, the MFS pore-water pressure model is less applicable to engineering projects because the parameters are not readily available without involving site-specific laboratory cyclic tests.

This paper describes the nonlinear effective stress finite element approach incorporated in the computer program VERSAT (Wu 1998). Major features of this approach include the use of a third parameter in the original two-parameter hyperbolic stress–strain model, a modified expression for unloading–reloading modulus in the MFS pore-water pressure model, and a third pore-water pressure model based on cyclic shear stress. The third pore-water pressure model uses the equivalent number of uniform cyclic shear stresses, originally proposed by Seed et al. (1976), for the assessment of pore-water pressure.

Dynamic analyses have been conducted to simulate the seismically induced soil liquefaction and ground deformation of the Upper San Fernando Dam under the 1971 San Fernando Earthquake. The analyses were conducted using the finite element computer program VERSAT. Soil liquefaction was assessed for each individual soil element. The effects of seismically induced pore-water pressures on soil stiffness and strength are also taken into account in the effective stress approach. Post-liquefaction strength and stiffness properties were applied to the liquefied elements. The permanent plastic deformation of the earth structures accumulates as soil elements liquefy during the earthquake and start to take on post-liquefaction residual strengths and reduced stiffness. The computed zones of liquefaction and deformation are compared with the measured response and with the results obtained by others.

## Performance of Upper San Fernando Dam under 1971 San Fernando Earthquake

The Upper San Fernando Dam, located northwest of Los Angeles and north of the Lower San Fernando Dam, was completed in 1922 using a semihydraulic fill technique (Seed et al. 1973). The dam was about 80 ft (24.4 m) high and was constructed upon 50 ft (15.2 m) of alluvial deposits overlying bedrock.

The 1971 San Fernando Earthquake had a moment magnitude of 6.7 and an epicentre about 13 km from the dam site. The peak horizontal acceleration at the dam site was estimated to be around 0.6*g*. Several longitudinal cracks were observed along almost the full length of the dam on the upstream slope slightly below the pre-earthquake reservoir level. Displacements of the dam observed immediately after the earthquake are shown in Fig. 1. The crest of the dam moved 4.9 ft (1.50 m) downstream and settled 2.5 ft (0.76 m). A 2 ft (0.61 m) high pressure ridge was also observed at the downstream toe. Sand boils below the toe and increased water levels in three standpipe piezometers suggested that soil liquefaction had occurred. Water overflowed from two of the piezometers.

The reservoir level at the time of earthquake was at elevation 1212 ft (369.51 m), 6 ft (1.83 m) below the crest of the dam.

## Soil stiffness and strength parameters of the Upper San Fernando Dam

In general, the low-strain shear modulus, $G_{max}$, can be determined from the in situ measured shear wave velocity, $V_s$, and the soil mass density, ρ, as follows:

$$[1] \qquad G_{max} = \rho V_s^2$$

In recognizing the increasing nature of shear modulus with increasing confining pressure, Seed and Idriss (1970) proposed a convenient relationship between the shear modulus and the confining stress. A modified form of the Seed and Idriss relationship is

© 2001 NRC Canada

**Fig. 2.** Finite element mesh showing soil material zones of the Upper San Fernando Dam.

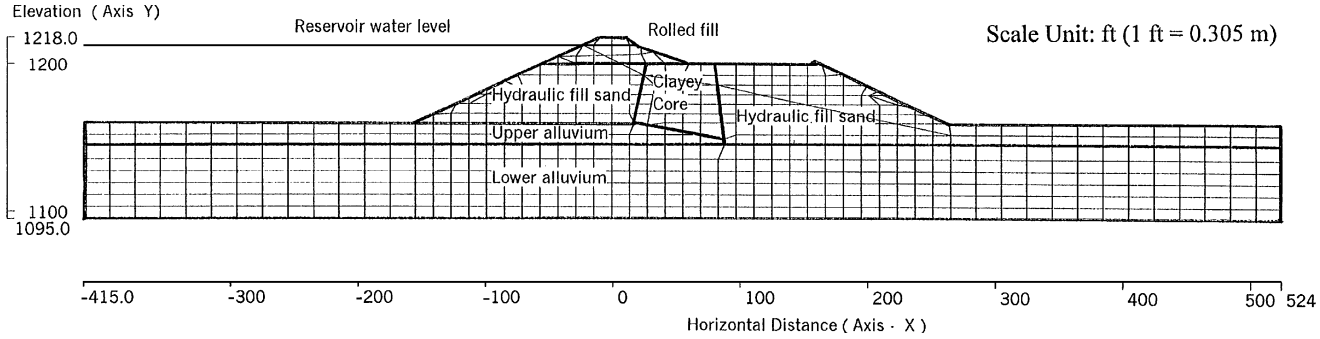


**Table 1.** Soil stiffness and strength parameters of the Upper San Fernando Dam (Seed et al. 1973).

| | | | Strength parameters | | Stiffness parameters* | | |
|---|---|---|---|---|---|---|---|
| Soil unit | Soil material | Unit weight (kN/m$^3$) | $c'$ (kPa) | $\phi'$ (°) | $K_{2max}$ | $K_g$ | $K_b$ |
| 1 | Rolled fill | 22.0 | 124.5 | 25 | 52 | 1128 | 2821 |
| 2 | Hydraulic fill | 19.2 | 0 | 37 | 30 | 651 | 1630 |
| 3 | Clay core | 19.2 | 0 | 37 | —† | 651 | 1630 |
| 4 | Upper alluvium | 20.3 | 0 | 37 | 40 | 868 | 2170 |
| 5 | Lower alluvium | 20.3 | 0 | 37 | 110 | 2387 | 6000 |

*Modulus exponents ($m = n = 0.5$) were used for all soil units.
†For the clay core, the low-strain shear modulus was suggested by Seed et al. (1973) as $G_{max} = 2300S_u$, with $S_u = 57.45$ kPa (1200 psf).

$$[2] \qquad G_{max} = 21.7K_{2max}P_a\left(\frac{\sigma'_m}{P_a}\right)^{0.5}$$

where $P_a$ is the atmospheric pressure, $\sigma'_m$ is the effective mean normal stress, and $K_{2max}$ is a soil modulus coefficient.

Seed et al. (1986) proposed that $K_{2max}$ can be correlated with the standard penetration resistance $(N_1)_{60}$. $K_{2max}$ can also be computed directly from the normalized shear wave velocity, $V_{s1}$, using the following equation:

$$[3] \qquad K_{2max} = \frac{0.0564\rho}{P_a}V_{sl}^2$$

where $V_{s1} = V_s/(\sigma'_{v0}/P_a)^{0.25}$, in which $\sigma'_{v0}$ is the effective vertical stress and $\sigma'_m = 0.67\sigma'_{v0}$ is used in the derivation of eq. [3].

Empirical relationships between $G_{max}$ and the confining pressure are also available based on the void ratio of sand (Hardin and Drnevich 1972). In the analyses using VERSAT, the shear modulus and bulk modulus are expressed in the following equations:

$$[4] \qquad G_{max} = K_gP_a\left(\frac{\sigma'_m}{P_a}\right)^n$$

$$[5] \qquad B = K_bP_a\left(\frac{\sigma'_m}{P_a}\right)^m$$

where $B$ is the bulk modulus, $K_g$ is the shear modulus constant, $n$ is the shear modulus exponent (normally $n = 0.5$), $K_b$ is the bulk modulus constant, and $m$ is the bulk modulus exponent.

Figure 2 shows the geometrical configuration and distribution of soil material zones used in the finite element analysis of the Upper San Fernando Dam. The dam section consists of five soil units as originally classified by Seed et al. (1973). The soil parameters associated with the five soil units are directly obtained from Seed et al. and listed in Table 1.

## Procedures for static stress analysis

A bilinear, elastic – perfectly plastic stress–strain relationship with a Mohr-Coulomb failure criterion has been used in the VERSAT static stress analyses. The elastic shear modulus $G$ and bulk modulus $B$ were used for simulating the linear stress–strain behavior. A friction angle and cohesion were used in the Mohr-Coulomb failure model. For the purpose of a static stress analysis, the elastic moduli can be estimated using typical values of elastic moduli under static loading conditions (Byrne et al. 1987) from the low-strain shear modulus.

The technique of layered construction was applied in the static stress analysis. Since VERSAT operates in an effective stress manner, the following procedures have been followed to model the static effective stress conditions:

(1) The upper and lower alluvium layers (Fig. 2) and part of the downstream hydraulic fill below elevation 1160 ft (the reservoir bed elevation) were first placed sequentially as nonsubmerged soil. This placement was comprised of eight vertical finite elements in Fig. 2.

(2) A water level, varying from elevation 1160 ft directly underneath the reservoir to elevation 1152 ft within the downstream hydraulic fill, was applied. The model was then brought to force equilibrium.

© 2001 NRC Canada

(3) Soil materials above elevation 1160 ft were divided into layers and placed sequentially as nonsubmerged soil. The water level remained unchanged.

(4) The water level was then raised to the reservoir water level within the pond and to the phreatic surface level within the dam body. Boundary water pressures were applied along the interior dam surface and the reservoir bed to account for water pressures. The water pressures were applied in the form of nodal forces. The new water level and the boundary water pressures were applied simultaneously in six increments to ensure a smooth transaction of effective stresses during the load application. In this way, effective stresses and static pore-water pressures are updated corresponding to the new water level.

(5) Layers above the final water level, such as the top layer of the rolled fill, were simply added without changing boundary pressures or nodal forces. Nodal forces and water levels specified in the previous steps of analyses are maintained.

## Hyperbolic nonlinear shear stress – shear strain relationship for dynamic analysis

Under cyclic loading, the plots of shear stress versus shear strain tend to form a hysteresis loop. The shape (slope) of the stress–strain loop determines the degree of reduction of shear modulus with shear strain, and the area of the hysteresis loop represents the amount of strain energy dissipated during the cycle of loading and unloading. The dissipated energy governs the degree of material damping at this strain level.

In a dynamic analysis involving hysteretic nonlinearity, a rigorous method of analysis for modeling the shear stress – shear strain behavior is to follow the actual loading–unloading–reloading hysteresis loop. A truly nonlinear stress–strain model will simulate both the reduction of shear modulus and the frequency-independent nature of hysteretic damping. This method of stress–strain modeling has been successfully applied in one-dimensional ground-motion analyses (Finn et al. 1977) and two-dimensional plane-strain analyses (Finn et al. 1986, 1999; Wu 1998; Gohl et al. 1997).

When the nonlinear hyperbolic model is used, shear stress – shear strain behavior of soil is modeled to be nonlinear and hysteretic and to exhibit the Masing behavior during unloading and reloading. The Masing behavior provides hysteretic damping.

The relationship between the shear stress, $\tau_{xy}$, and the shear strain, $\gamma$, for the initial loading condition is assumed to be hyperbolic. This relationship is given by

$$[6] \qquad \tau_{xy} = \frac{G_{\max}\gamma}{1 + \frac{G_{\max}}{\tau_{\text{ult}}}|\gamma|}$$

where $\tau_{\text{ult}}$ is the ultimate shear stress in the hyperbolic model.

The Masing criterion has been used to simulate the unloading–reloading behavior. A more detailed description of this nonlinear stress–strain model can be found in Finn et al. (1977). The extended application of the Masing criterion to irregular loading such as earthquake loading was also presented by Finn et al. In VERSAT, the ultimate shear stress in the hyperbolic model is calculated using the following equation:

$$[7] \qquad \tau_{\text{ult}} = \frac{G_{\max}}{R_{\text{f}}}$$

where $R_{\text{f}}$ is a modulus reduction factor.

The shear strength, $\tau_{\text{f}}$, of a soil element is calculated using

$$[8] \qquad \tau_{\text{f}} = 0.5(\sigma'_x + \sigma'_y)\sin(\phi') + c'\cos(\phi')$$

where $\sigma'_x$ and $\sigma'_y$ are the current effective normal stresses, and $c'$ and $\phi'$ are the drained strength parameters of soil.

Equation [7] allows a specified shear modulus reduction curve and damping curve to be matched at the strain range of interest by using the hyperbolic model with an appropriate $R_{\text{f}}$ factor. The shear modulus reduction curve represents the relationship between the secant shear modulus, which is widely used in an equivalent linear analysis as SHAKE (Schnabel et al. 1972) and is represented as a fraction of the low-strain shear modulus, and the level of shear strain.

The modulus reduction curves and damping curves implied in a hyperbolic model are shown in Fig. 3 for various values of $R_{\text{f}}$. In general, a larger $R_{\text{f}}$ represents more reduction in shear modulus and more damping and vice versa. Modulus reduction curves and damping curves commonly used in the SHAKE analyses are also shown in Fig. 3 for comparison. For shear strains ranging from 0.01 to 0.05%, the hyperbolic model with the Masing rule can well simulate the hysteretic behavior of sand using an $R_{\text{f}}$ value of 1500–2000. The modulus reduction and damping implied in the hyperbolic model are within the range of values for sand. For shear strains ranging from 0.05 to 0.2%, the modulus reduction curve can still be followed using the hyperbolic model with an $R_{\text{f}}$ value of 1500, but the damping implied in the hyperbolic model ($R_{\text{f}}$ = 1500) exceeds the average damping values for sand (Seed et al. 1986). At a shear strain level of 0.2%, the damping of the hyperbolic model ($R_{\text{f}}$ = 1500) is about 50% higher than the average damping of sand. For this range of strain, an $R_{\text{f}}$ value of 1000 is more appropriate for damping simulation (Fig. 3).

The hysteretic damping implied in the hyperbolic model with the Masing rule is too high when the shear strain is greater than 0.5% for all values of $R_{\text{f}}$ presented in Fig. 3 and thus its application should be limited to the understanding of this limitation in the hyperbolic model.

The nonlinear hyperbolic model is considered to be a more precise method for modeling soil nonlinearity in comparison with the equivalent linear method of the SHAKE type. The equivalent linear method simply uses a constant shear strain applied to the entire duration of earthquake shaking. The nonlinear analysis using the hyperbolic model has the advantage of modeling soil hysteretic behavior for each individual cycle of earthquake shaking having different strain amplitudes and thus different moduli and damping values. The strain limits of the hyperbolic model as discussed earlier are applicable to an ideal shear stress – shear strain hysteresis loop. The strain limits are not the total strain of a soil element when the origin of a stress–strain loop has moved away from its original origin as permanent displacements (strains) accumulate.

© 2001 NRC Canada

**Fig. 3.** Secant shear modulus and damping ratios for various values of $R_f$ in a hyperbolic model.

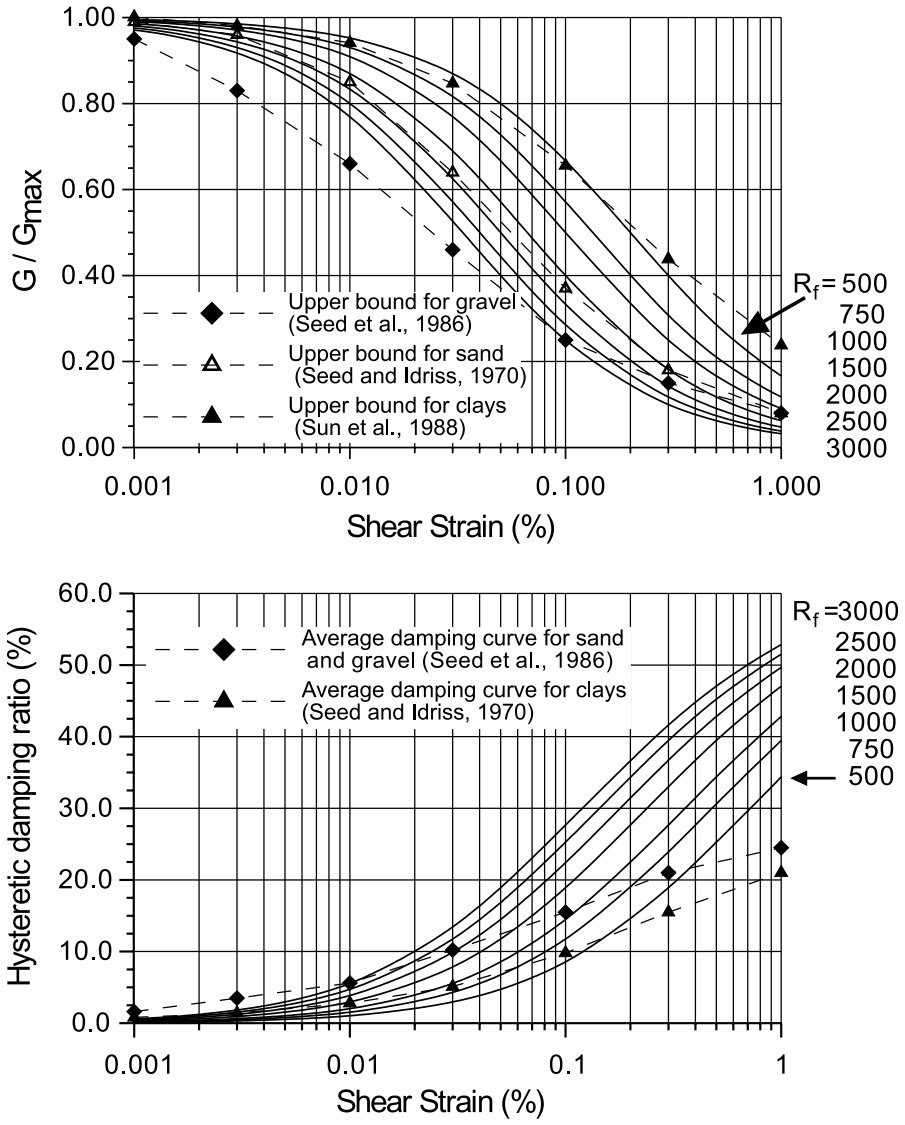


## Pore-water pressure models

The residual pore-water pressures are due to plastic deformations in the sand skeleton. They persist until dissipated by drainage or diffusion. Therefore they provide a great influence on the strength and stiffness of the sand skeleton. The shear moduli ($G_{max}$) and the ultimate shear stresses ($\tau_{ult}$) in eq. [6] are very much dependent on the current effective stresses in the soil. Hence during an analysis, excess pore-water pressures must be continuously updated and their effects on moduli must be continuously taken into account. The effects of pore-water pressures on $G_{max}$ and $\tau_{ult}$ are quantified in a later section.

Three models are available in VERSAT for computing the excess pore-water pressures. The first model was the Martin–Finn–Seed (MFS) model developed by Martin et al. (1975). The second model is a modification of the MFS model proposed by Wu (1996). Both models use cyclic shear strains to calculate the excess pore-water pressures induced by cyclic loads. The third model was developed by Seed et al. (1976). This model determines the excess pore-water pressures based on the equivalent number of uniform cyclic shear stress cycles. Features of each pore-water pressure model are briefly described in the following sections.

### Martin–Finn–Seed (MFS) pore-water pressure model

The increments in pore-water pressure $\Delta u$ that develop in saturated soil under seismic shear strains are related to the plastic volumetric strain increments $\Delta\varepsilon_v^p$ that occur in the same sand under drained conditions with the same shear strain history. For saturated sand in undrained conditions, water may be assumed to be effectively incompressible compared with the sand skeleton. Thus under conditions of zero volume change Martin et al. (1975) proposed the following relationship for computing the pore-water pressure increment $\Delta u$:

$$[9] \qquad \Delta u = E_r \Delta\varepsilon_v^p$$

where $\Delta\varepsilon_v^p$ is the plastic volumetric strain increment accumulated during a period of strain history, $\Delta u$ is the residual pore-water pressure increment, and $E_r$ is the unloading–

© 2001 NRC Canada

**Fig. 4.** Relationship between plastic volumetric strain and number of shear strain cycles in the MFS pore-water pressure models.

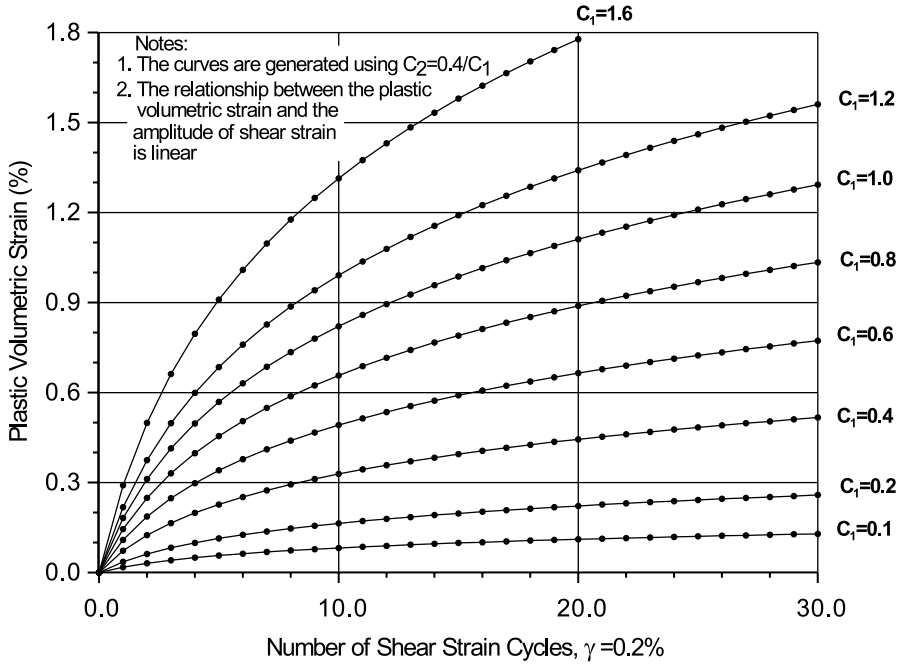


reloading modulus of the sand skeleton for the current effective stress level (Martin et al. 1975).

Under harmonic loads, $\Delta\varepsilon_v^p$ is usually accumulated at each cycle or at each half cycle of strain. Under irregular earthquake loads, $\Delta\varepsilon_v^p$ may be accumulated at points of strain reversal. After the potential volumetric strain is calculated, the increment in pore-water pressure $\Delta u$ can be determined from the unloading–reloading modulus of the sand skeleton $E_r$.

The volumetric strain increment, $\Delta\varepsilon_v^p$, is a function of the total accumulated volumetric strain, $\varepsilon_v^p$, and the amplitude of the current shear strain, $\gamma$ (Martin et al. 1975). Byrne (1991) modified the original four-parameter expression of the volumetric strain increment of Martin et al. (1975) and proposed the following two-parameter relationship:

$$[10] \qquad \Delta\varepsilon_v^p = C_1\gamma \exp\left(-C_2\frac{\varepsilon_v^p}{\gamma}\right)$$

where $C_1$ and $C_2$ are the volumetric strain constants. The relationship between $\Delta\varepsilon_v^p$ and the shear strain in eq. [10] was developed for a simple shear type of one-dimensional loading condition. For the two-dimensional strain condition such as the analysis of a dam, the shear strain in the horizontal plane, $\gamma_{xy}$, is used as the shear strain in eq. [10] for simplicity. Although the shear strain in the horizontal plane may not be the maximum shear strain of a soil element under two-dimensional strain conditions, this assumption is considered appropriate for engineering practice.

The relationship between plastic volumetric strain and number of shear strain cycles in the MFS model is illustrated in Fig. 4 for a strain amplitude of 0.2%. The following equation was given by Martin et al. (1975) to calculate the unloading–reloading modulus:

$$[11] \qquad E_r = \frac{(\sigma'_v)^{1-m}}{mK_2(\sigma'_{v0})^{n-m}}$$

where $\sigma'_v$ is the current effective vertical stress ($\sigma'_v = \sigma'_{v0} - u$); $u$ is the current excess pore-water pressure; and $K_2$, $m$, and $n$ are experimental constants derived from unloading–reloading tests (Bhatia 1980). Without experimental data, determination of constants $K_2$, $m$, and $n$ is not straightforward.

**Modified MFS pore-water pressure model**

Wu (1996) proposed that the unloading–reloading modulus, $E_r$, be determined according to the current effective vertical stress $\sigma'_v$ using the following equation:

$$[12] \qquad E_r = M\sigma'_v$$

where $M$ is the unloading–reloading modulus constant.

The determination of the unloading–reloading modulus constant, $M$, is based on the volume-constant concept that there is a unique relationship between the relative density of sand and the amount of potential volumetric strain required to trigger initial liquefaction. Ishihara and Yoshimine (1992) stated that "the volume change characteristics of sand during re-consolidation following the cyclic loading is uniquely correlated with the amount of developed pore water pressure, no matter what types of irregular loads are used, and irrespective of whether the irregular load is applied in one-direction or in multi-directional manner." Their work strongly supports the concept that at a specific relative density the sample will experience initial liquefaction if a certain amount of potential volumetric strain (referred to by Ishihara and Yoshimine as volume change during reconsolidation following the cyclic loading) is developed in the sample.

Relationships between the pore-water pressure ratios and the plastic volumetric strains for various values of $M$ are

© 2001 NRC Canada

**Fig. 5.** Relationship between pore-water pressure ratios (PPR) and plastic volumetric strain in the modified MFS pore-water pressure model.

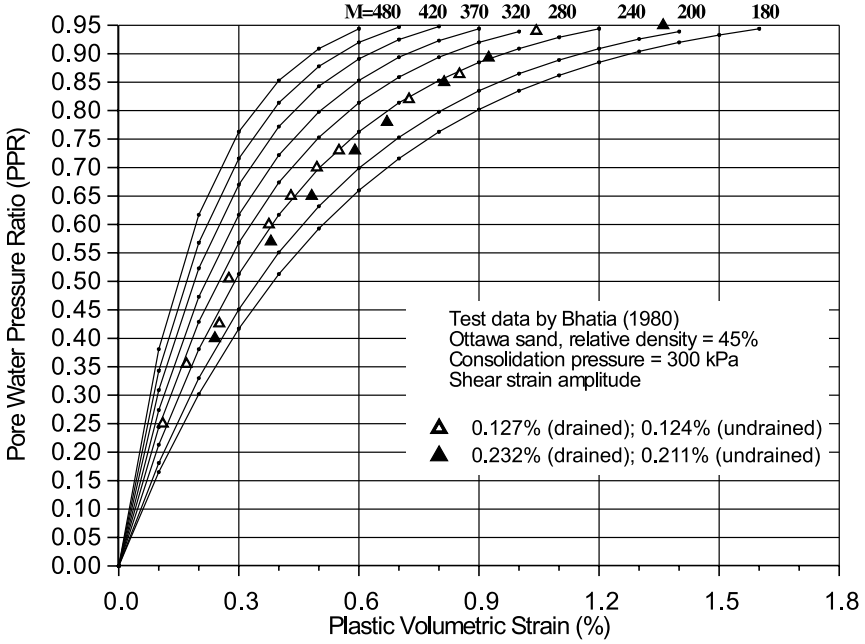


shown in Fig. 5. Laboratory tests should be conducted to derive the unloading–reloading modulus constant, $M$. In the absence of experimental data, the following equation may be used for estimating $M$:

$$[13] \quad M = 10(N_1)_{60} + a$$

where $a$ is a constant ranging from 150 to 180, and $(N_1)_{60}$ is the standard penetration resistance and is related to sand density. An upper bound value of $M$ is limited to 480.

The modified MFS pore-water pressure model was developed by Wu (1996) using test data of Bhatia (1980). The pore-water pressures computed using the modified MFS model are compared with the measured pore-water pressures in Fig. 5 for a sample of Ottawa sand having a relative density of 45%. The computed pore-water pressures agree with the measured pore-water pressures at all levels of strain using $M = 240$.

**Seed et al. pore-water pressure model**

The model proposed by Seed et al. (1976) uses the equivalent number of uniform stress cycles for the assessment of pore-water pressure. The seismically induced pore-water pressures are computed using the following relationship (Seed et al. 1976):

$$[14] \quad \frac{u}{\sigma'_{v0}} = \frac{2}{\pi}\arcsin\left(\frac{N_{15}}{N_1}\right)^{\frac{1}{2\theta}}$$

where $\theta$ is an empirical constant; $N_1$ is the number of uniform shear stress cycles that cause liquefaction ($N_1 = 15$ used in VERSAT); and $N_{15}$ is the equivalent number of uniform shear stress cycles, and

$$[15] \quad N_{15} = \Sigma N_{15(1)}$$

The following equation is proposed to convert shear stresses of irregular amplitudes to uniform shear stress cycles:

$$[16] \quad N_{15(1)} = \left(\frac{\tau_{cyc}}{\tau_{15}}\right)^{\alpha}$$

where $\tau_{15}$ is the shear stress required to cause liquefaction in 15 cycles, $\tau_{cyc}$ is the cyclic shear stress of any amplitude, $N_{15(1)}$ is the equivalent number of cycles corresponding to $\tau_{15}$ for one cycle of $\tau_{cyc}$, and $\alpha$ is a shear stress conversion constant.

The number of cycles required to cause liquefaction at a cyclic shear stress level of $\tau_{cyc}$ is expressed as

$$[17a] \quad 15 = N_{cyc}\left(\frac{\tau_{cyc}}{\tau_{15}}\right)^{\alpha}$$

$$[17b] \quad \frac{\tau_{cyc}}{\tau_{15}} = \left(\frac{15}{N_{cyc}}\right)^{\frac{1}{\alpha}}$$

where $N_{cyc}$ is the number of cycles to cause initial liquefaction at $\tau_{cyc}$. There are abundant test data showing the relationship between the cyclic shear stress and the number of cycles to initial liquefaction. Curves corresponding to different values of $\alpha$ in eq. [17*b*] are shown in Fig. 6*a*. Test data from Seed et al. (1973) for the hydraulic fill of the Upper San Fernando Dam are also plotted in Fig. 6*a*. A value of $\alpha = 3.0$ was found appropriate to fit the test data of Seed et al. for the Upper San Fernando Dam and was thus used in the analysis.

*Relationship between $K_M$ and $\alpha$ in the Seed et al. pore-water pressure model*

In a simplified liquefaction assessment (Seed and Harder 1990) recommended by the National Center for Earthquake Engineering Research (NCEER) (Youd and Idriss 1997), the relationship between the cyclic shear stress and the number of cycles to initial liquefaction in eq. [17*b*] is alternatively

© 2001 NRC Canada

**Table 2.** Relationship between earthquake magnitude, number of representative cycles, and scaling factors.

| Earthquake magnitude | No. of representative cycles at $\tau_{cyc}$, $N_M$ (Seed et al. 1975) | Scaling factor, $K_M$ (Seed and Idriss 1982) | NCEER scaling factor, $K_M$ (Youd and Idriss 1997) |
|---|---|---|---|
| 5.25 | 2–3 | 1.43 | 2.2–2.8* |
| 6 | 5 | 1.32 | 1.76–2.1 |
| 6.75 | 10 | 1.13 | 1.31–1.42 |
| 7.5 | 15 | 1.0 | 1.0 |
| 8.5 | 26 | 0.89 | 0.72 |

* Corresponding to magnitude 5.5.

expressed using the relationship between the magnitude scaling factor, $K_M$, and the earthquake magnitude (represented by $N_M$):

$$[18] \quad K_M = \left(\frac{15}{N_M}\right)^{\frac{1}{\alpha}}$$

where $N_M$ is the number of representative cycles corresponding to earthquake magnitude.

The number of representative cycles, $N_M$, for various earthquake magnitudes was originally proposed by Seed et al. (1975). The earthquake magnitude scaling factor, $K_M$, was then introduced by Seed and Idriss (1982) and thereafter studied by many other researchers. Ranges of $K_M$ recommended by the NCEER (Youd and Idriss 1997) are shown in Fig. 6*b* and summarized in Table 2. Using the representative number of cycles of Seed et al., curves corresponding to different values of $\alpha$ in eq. [18] are plotted in Fig. 6*b* for comparison with test data. Figure 6*b* shows that $\alpha = 1.5$ results in a $K_M$–magnitude relationship in good agreement with NCEER recommendations. The $K_M$–magnitude relationship of Seed and Idriss (1982) can be represented by an $\alpha$ value greater than 3.

*Definition of $\tau_{15}$ in the Seed et al. pore-water pressure model*

The shear stress to cause liquefaction in 15 cycles, $\tau_{15}$, is calculated using the following equation:

$$[19] \quad \tau_{15} = \text{CRR}\ K_\sigma K_\alpha \sigma'_{v0}$$

Corrected blow counts, $(N_1)_{60}$, can be used for evaluating the cyclic resistance ratio, CRR, for clean sand at an overburden stress of 96 kPa (2000 pounds per square foot (psf)) using the modified Seed curve recommended by the NCEER (Youd and Idriss 1997).

The correction factor, $K_\sigma$, was then applied to adjust CRR to in situ effective overburden stresses using the NCEER (Youd and Idriss 1997) recommended curve.

The correction factor for static shear stress, $K_\alpha$, is simply considered as unity in the analysis. Although the dynamic analysis starts from the static shear stress point, it is not certain if the method of analysis has included the effect of static shear stress on liquefaction resistance.

*Factor of safety against liquefaction*

From eq. [16] the equivalent number of cycles, $N_{15}$, corresponding to $\tau_{15}$ for 15 cycles of $\tau_{cyc}$ is

**Fig. 6.** (*a*) Normalized cyclic stress ratios. (*b*) Magnitude scaling factors for various values of $\alpha$ in eq. [16].

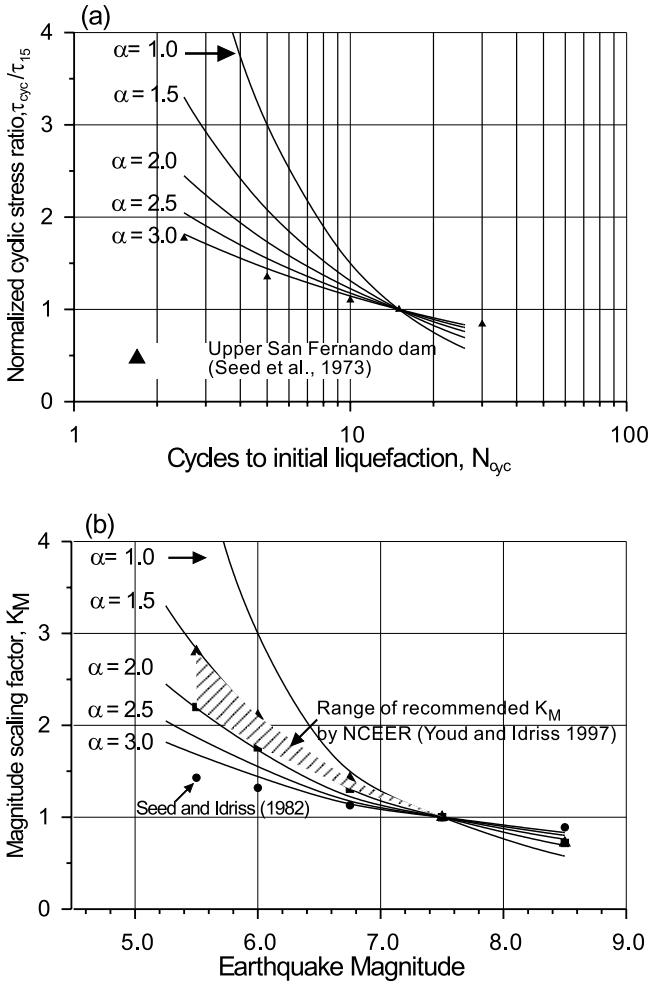


$$[20a] \quad N_{15} = 15\left(\frac{\tau_{cyc}}{\tau_{15}}\right)^{\alpha}$$

Then the factor of safety ($FS_{liq} = \tau_{15}/\tau_{cyc}$) against soil liquefaction can be calculated, according to the definition used in Seed and Harder (1990), using the following equation:

$$[20b] \quad FS_{liq} = \left(\frac{15}{N_{15}}\right)^{\frac{1}{\alpha}}$$

© 2001 NRC Canada

**Table 3.** Pore-water pressure parameters and residual strengths used in the modified MFS model.

| Material No. | Soil description | $C_1$ | $C_2$ | $M$ | Residual strength (kPa)* | $K_cLIQ$ | Equivalent $(N_1)_{60}$ |
|---|---|---|---|---|---|---|---|
| 2a | Upstream hydraulic fill | 0.32 | 1.25 | 320 | 23.0 (480) | 400 | 14 |
| 2b | Downstream hydraulic fill | 0.32 | 1.25 | 320 | 23.0 (480) | 400 | 14 |
| 2c | Hydraulic fill in the downstream free field | 0.32 | 1.25 | 320 | 14.4 (300) | 400 | 14 |

* Pounds per square feet in parentheses.

**Table 4.** Pore-water pressure parameters and residual strengths used in Seed et al. (1976) pore-water pressure model.

| Material No. | Soil description | Equivalent $(N_1)_{60}$ | CRR | $\alpha$ | $\theta$ | Residual strength (kPa)* | $K_cLIQ$ |
|---|---|---|---|---|---|---|---|
| 2a | Upstream hydraulic fill | 14 | 0.154 | 3.0 | 0.1 | 23.0 (480) | 400 |
| 2b | Downstream hydraulic fill | 14 | 0.154 | 3.0 | 0.1 | 23.0 (480) | 400 |
| 2c | Hydraulic fill in the downstream free field | 14 | 0.154 | 3.0 | 0.1 | 14.4 (300) | 400 |

* Pounds per square feet in parentheses.

## Strain-softening effects of soils

A key feature of the effective stress analysis is that it allows some elements to liquefy first and others to liquefy at a later time. By doing this, the earlier liquefied soil elements exhibit a softened response that creates an isolation effect for shaking of soil elements above them. The cyclic shear stress history of elements in the upper layers may therefore be significantly affected by the liquefied soil elements below them.

In an effective stress analysis, the drained strength parameters are used in the analysis. The effect of excess pore-water pressure on shear strength is considered by reduced effective stresses. The effect of excess pore-water pressure on shear stiffness is considered by a reduced shear modulus and ultimate shear stress as follows:

$$[21] \quad G_0 = G_{max}\sqrt{\frac{\sigma'_v}{\sigma'_{v0}}}$$

$$[22] \quad \tau_0 = \tau_{ult}\frac{\sigma'_v}{\sigma'_{v0}}$$

where $G_0$ is the updated initial shear modulus for the hyperbolic model, and $\tau_0$ is the updated ultimate shear stress for the hyperbolic model. The lower bound value of $\tau_0$ is the residual strength, and the lower bound value of $G_0$ is the shear modulus of the liquefied soil.

## Modeling of post-liquefaction behavior of soil

Residual strength, $S_{ur}$, and stiffness were assigned to liquefied soil materials during dynamic analysis at the time when liquefaction was triggered. Residual strength of liquefied materials has a major impact on the post-liquefaction stability of an earth structure. The selection of residual strength remains a very controversial issue, as discussed by Finn (1998). Residual strengths are often obtained from back analysis of case histories (Seed and Harder 1990) or from direct laboratory tests. Back analysis of the Upper San Fernando Dam indicated an average residual strength of 28.7 kPa (600 psf) for the liquefied loose hydraulic fill sand (Seed and Harder 1990).

In VERSAT, the post-liquefaction stress and strain relationship is also defined by a hyperbolic curve using an initial shear modulus, $G_{liq}$, and the residual strength, $S_{ur}$. The relationship between $G_{liq}$ and $S_{ur}$ is defined by the following equation:

$$[23] \quad G_{liq} = K_cLIQ\ S_{ur}$$

where $K_cLIQ$ is a parameter defining the stiffness of liquefied soil. Once liquefaction is triggered in a soil element, the stiffness and strength are governed by the assigned stiffness $G_{liq}$ and shear strength $S_{ur}$ of liquefied soil. At this phase of analysis, the response of the liquefied soil elements is controlled by the total stress soil parameters that are not dependent on the pore-water pressures.

## Pore-water pressure parameters and residual strengths of the Upper San Fernando Dam

In the analysis the saturated hydraulic fills were divided into three zones, the upstream fill with distances $X < 50$ ft in Fig. 2, the downstream fill with $50 < X < 250$ ft, and the downstream fill in the free field with $X > 250$ ft. The soil parameters related to soil liquefaction for the three zones are summarized in Table 3 for the modified MFS pore-water pressure model. The values of volumetric strain constants $C_1$ and $C_2$ were derived from the equivalent $(N_1)_{60}$ using Byrne (1991). A residual strength of 23 kPa (480 psf) was assigned to the hydraulic fill of the dam based on the review of blow count. However, this value of 23 kPa was considered too high for the hydraulic fill in the downstream free field where the effective overburden stresses are less than about 58 kPa. A lower residual strength of 14.4 kPa (300 psf) was used in this zone.

The soil parameters related to liquefaction used in the Seed et al. (1976) pore-water pressure model are listed in Table 4. The use of $\theta = 0.1$ in the analysis implies that the increase of pore-water pressure with an increase in the number of cyclic loads is very slow until the ratio of $N_{15}/N_l$ exceeds about 0.8. The pore-water pressure increases very quickly

© 2001 NRC Canada

**Fig. 7.** Zones of liquefaction (solid areas) of the Upper San Fernando Dam predicted using the modified MFS pore-water pressure model.

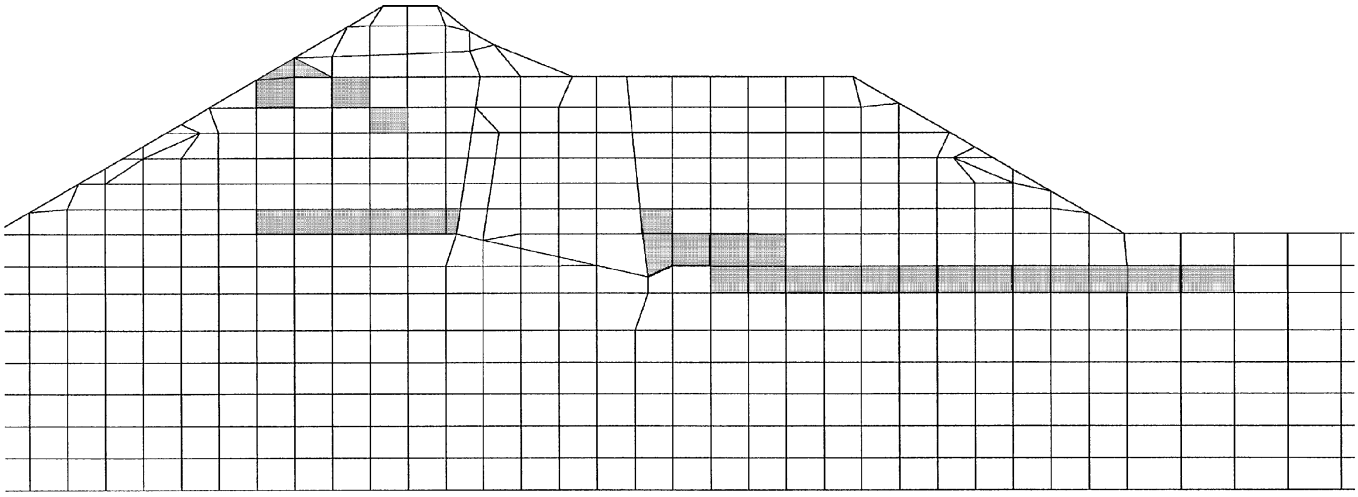

**Fig. 8.** Values of pore-water pressure ratios of the Upper San Fernando Dam predicted using the modified MFS pore-water pressure model.

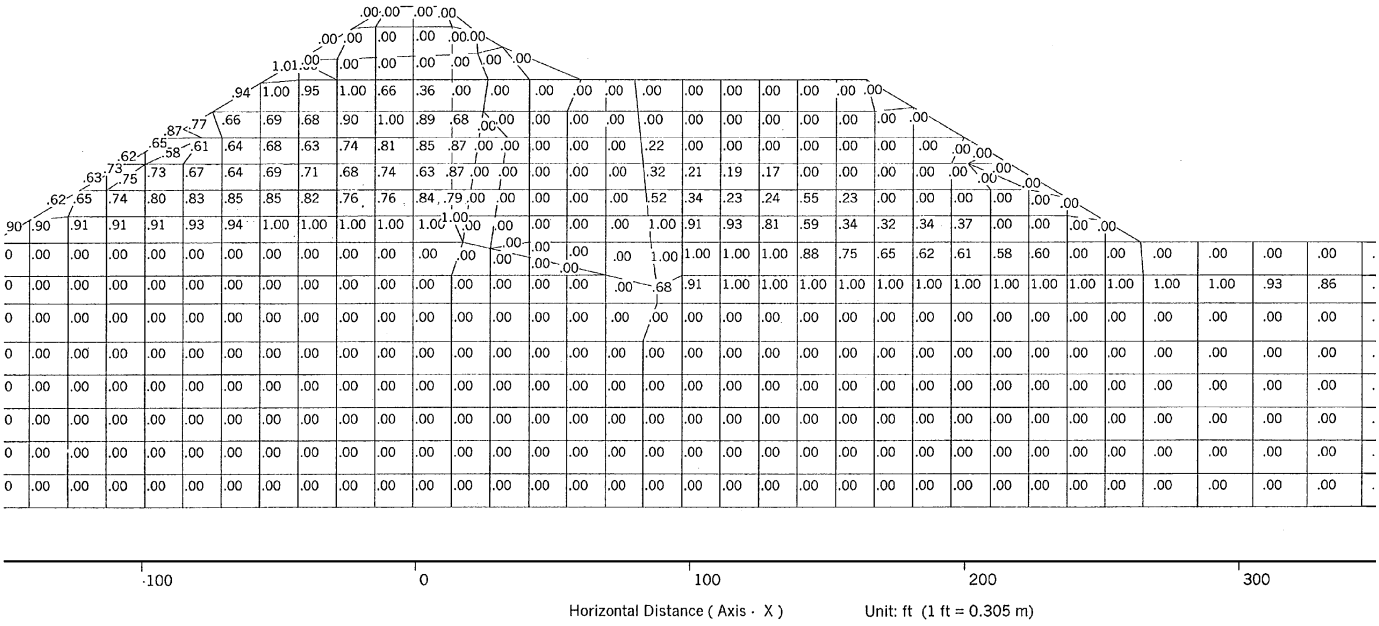


as the ratio $N_{15}/N_1 > 0.8$ (Seed et al. 1976). Use of a lower θ value represents a more conservative approach in terms of liquefaction assessment. However, it may result in a pore-water pressure that is too low for a nonliquefied soil element.

## Results of earthquake deformation analyses using the modified MFS model

The modified Pacoima dam accelerogram as originally used by Seed et al. (1973) was used in the dynamic analysis. The record has a peak acceleration of 0.6*g* and was applied as a rigid base motion at the base of the model shown in Fig. 1.

The zones of liquefaction for the modified MFS pore-water pressure model are shown in Fig. 7. Liquefaction was considered to occur when the pore-water pressures exceed 95% of the effective vertical stresses. The pore-water pressure ratio, PPR, is defined as

$$[24] \quad \text{PPR} = \frac{u}{\sigma'_{v0}}$$

where $u$ is the excess pore-water pressure induced by the earthquake excitation.

Values of pore-water pressure ratios developed in the hydraulic fill sands are shown in Fig. 8. The rolled fill cap, the clayey core, and the alluvium were not considered to develop any significant amount of pore-water pressure under the cyclic loads and therefore were not modeled for pore-water pressures in the analysis.

The results of the analysis show that the lower part, from elevation 1145 ft (349.1 m) to 1160 ft (353.7 m), of the downstream saturated hydraulic fill sand liquefied and liquefaction extended to the free field about 40 ft (12.2 m) away from the downstream toe. The upstream hydraulic fill sand liquefied mainly in the layer from elevation 1160 ft (353.7 m) to 1167 ft (355.8 m), with some zones of liquefaction between elevation 1185 ft (361.3 m) and elevation 1200 ft (365.9 m).

© 2001 NRC Canada

**Fig. 9.** Computed shear stress – shear strain response and pore-water pressure ratios at elements 369 and 490 of the Upper San Fernando Dam.

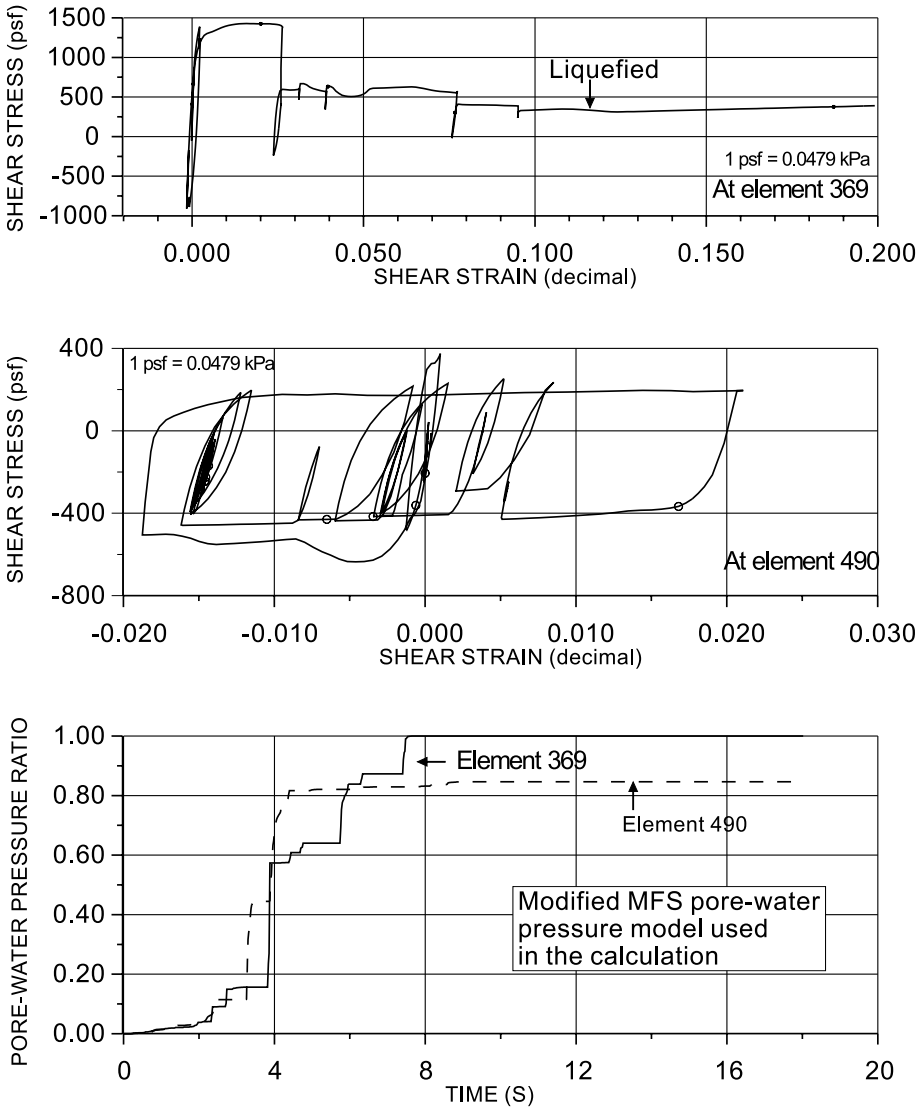


The extent of liquefaction in the upstream hydraulic fill is less than that in the downstream hydraulic fill sand (Fig. 7). However, the pore-water pressure ratios in the nonliquefied soil elements are in general high, in the range between 60 and 90%, in the upstream hydraulic fill. The pore-water pressure ratios in the nonliquefied soil elements on the downstream side are in general less than 50% (Fig. 8). The extent of liquefaction agrees, in general, with that assessed by Seed et al. (1973).

The shear stress – shear strain response curves at a nonliquefied upstream element (element 490 shown in Fig. 1) and at a liquefied downstream element (element 369 shown in Fig. 1) are shown in Fig. 9. The pore-water pressure ratios at the two elements are also shown in Fig. 9. The shear stress – shear strain relationship shows a stiff response at the beginning of the earthquake. This response relates to a low pore-water pressure as expected. The shear stress – shear strain response becomes softer when the pore-water pressure increases as shaking continues. Element 369 liquefied at about 7.5 s of earthquake shaking. When a soil element liquefies, the shear stress maintains at a constant level corresponding to residual strengths as specified (element 369). The nonliquefied soil element (element 490) showed a strain-softening response due to the development of pore-water pressure.

The computed deformations at the end of the earthquake are shown in Fig. 10 and indicate that the dam crest moved 4.9 ft (1.5 m) downstream and settled 2.4 ft (0.73 m), compared with measured deformations of 4.9 ft (1.5 m) and 2.5 ft (0.76 m), respectively. The computed deformations agree very well with the measured deformations.

Displacements along the dam surface computed by VERSAT are compared with those computed by FLAC (Itasca Consulting Group, Inc. 1998) in Fig. 11. The horizontal and vertical displacements computed by VERSAT agree well with the measured values from the dam crest to the edge of the downstream slope. In the same area, the horizontal displacements computed by Beaty and Byrne (1999), who used FLAC in a total stress approach, are in general less than the measured values. The dam crest was predicted by Beaty and Byrne to move about 2.7 ft (0.82 m) downstream

© 2001 NRC Canada

**Fig. 10.** Deformation pattern of the Upper San Fernando Dam predicted using the modified MFS pore-water pressure model.

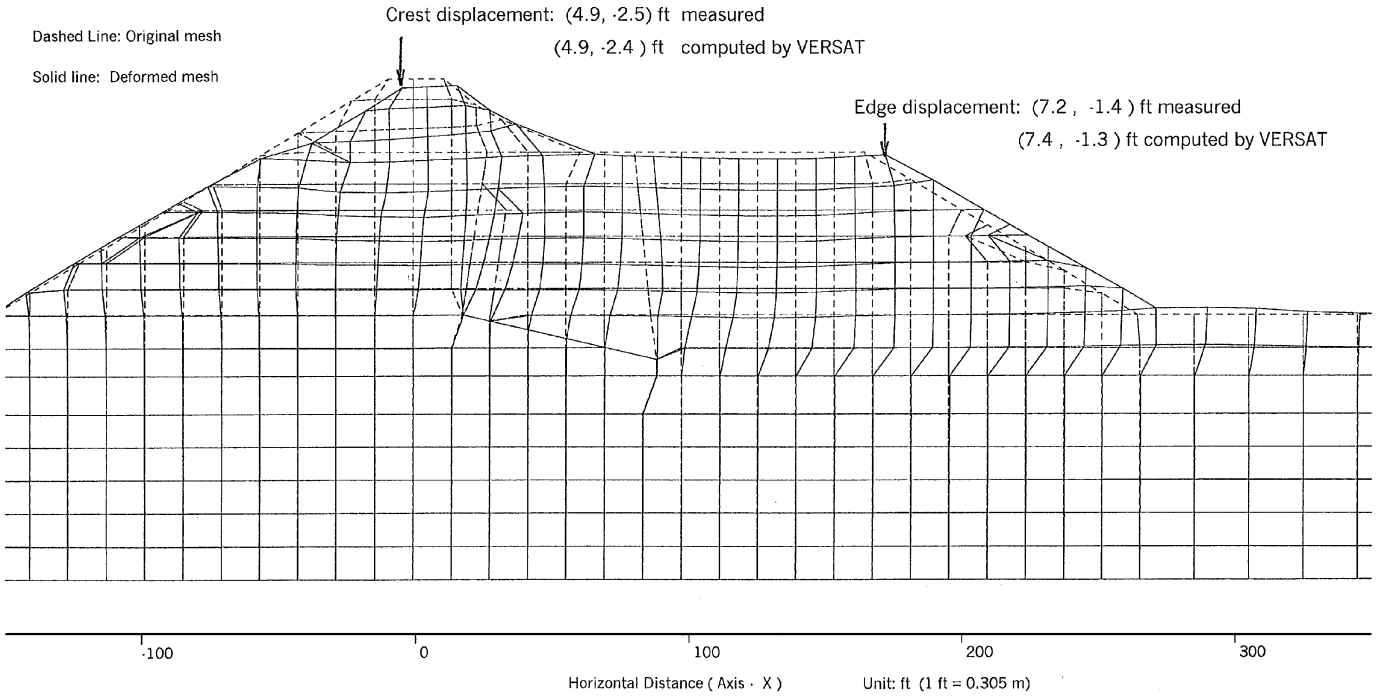


and settle 1.0 ft (0.30 m), compared with measured values of 4.9 ft (1.50 m) and 2.5 ft (0.76 m), respectively. The prediction by Moriwaki et al. (1998), who attempted a FLAC analysis in an effective stress approach, showed that the dam crest moved 2.3 ft (0.70 m) upstream and settled 3.7 ft (1.12 m). The direction of horizontal movement at the dam crest predicted by Moriwaki et al. disagrees with the observed direction of horizontal movement.

In the area from the edge to the toe of the downstream slope, the horizontal displacements predicted by both VERSAT and FLAC are in general 1–2 ft (0.30–0.61 m) greater than the measured displacements. VERSAT predicted a heaving displacement up to 1.5 ft (0.46 m) at the toe. FLAC analysis (Beaty and Byrne 1999) showed up to 0.3 ft (0.09 m) of heave at the toe.

## Results of earthquake deformation analyses using the Seed et al. pore-water pressure model

The zones of liquefaction for the Seed et al. (1976) pore-water pressure model are shown in Fig. 12. The extent of liquefaction induced by the model is much larger than that induced by the modified MFS model. The liquefied zone in the downstream agrees in general with Seed et al. (1973) liquefaction assessment. However, this study using the Seed et al. (1976) pore-water pressure model predicted much more liquefaction in the upstream hydraulic fill. Seed et al. (1973) predicted no liquefaction beyond about 80 ft (24.4 m) upstream of the dam centreline. This analysis showed liquefaction to the upstream toe about 155 ft (47.3 m) upstream of the dam centreline. The excessive extent of liquefaction in the upstream may be caused by a relatively low effective vertical stress in the area close to the upstream dam toe.

**Fig. 11.** Comparison of displacements along the dam surface.

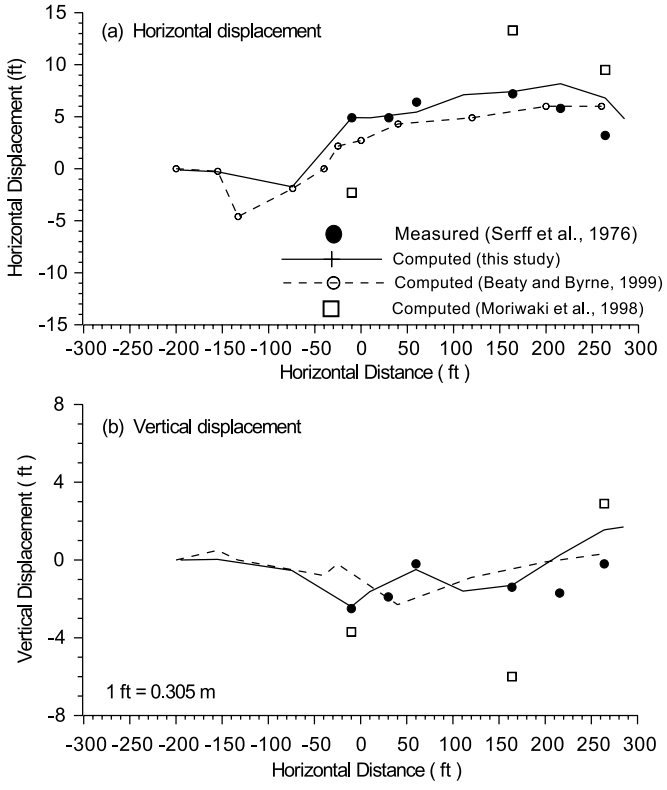


The computed deformations at the end of earthquake using the Seed et al. (1976) pore-water pressure model are shown in Fig. 13. The dam crest is predicted to move 2.0 ft (0.61 m) and settle 1.1 ft (0.34 m). The edge of the downstream slope is predicted to move 6.6 ft (2.01 m) downstream and settle 1.2 ft (0.37 m). The analysis underpredicted both

© 2001 NRC Canada

**Fig. 12.** Zones of liquefaction (solid areas) of the Upper San Fernando Dam predicted using the Seed et al. (1976) pore-water pressure model.

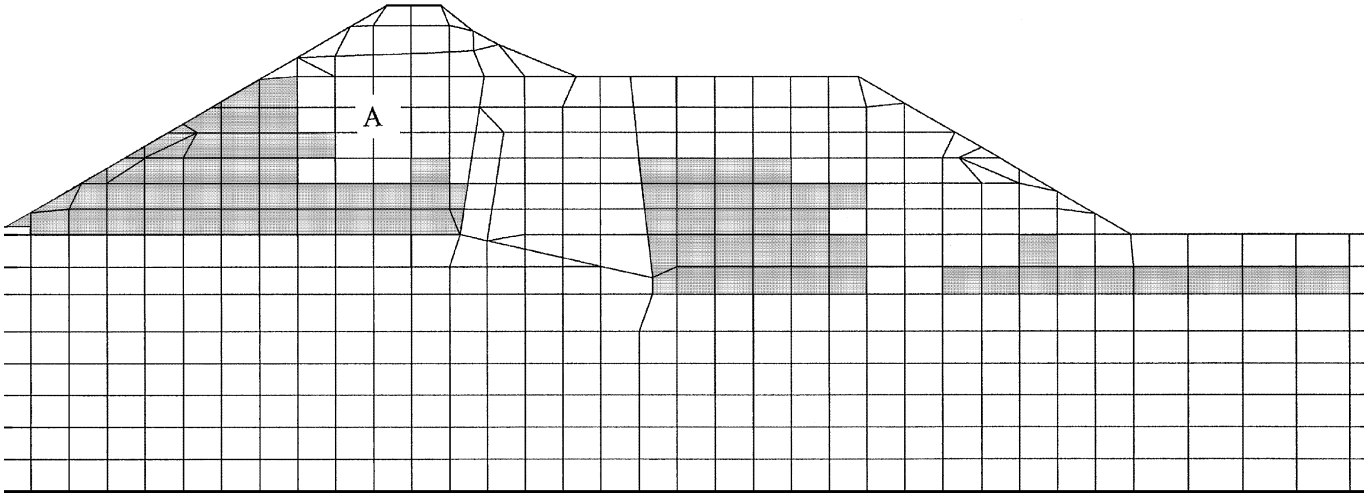


**Fig. 13.** Deformation pattern of the Upper San Fernando Dam predicted using the Seed et al. (1976) pore-water pressure model.

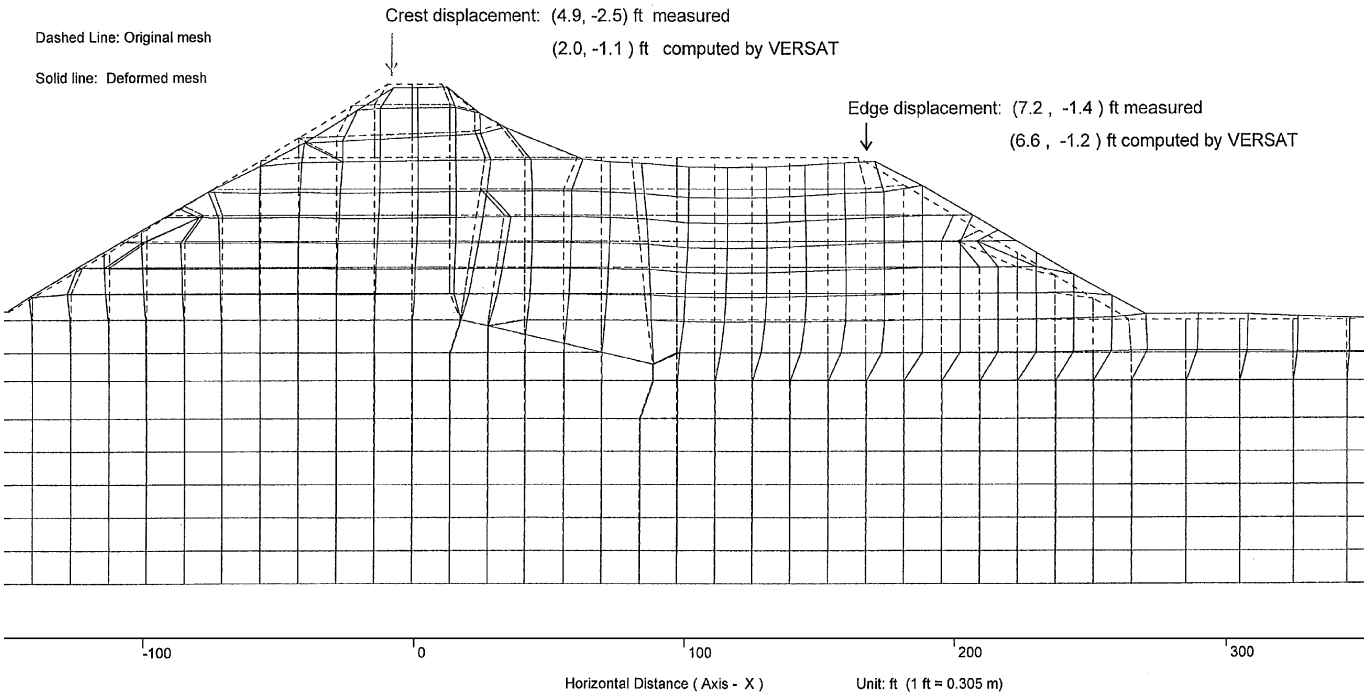


horizontal and vertical displacement at the dam crest. The computed deformations at the edge of the downstream slope agree well with the observed deformations. The deformation pattern predicted using the Seed et al. pore-water pressure model in this study is somewhat similar to that predicted by Beaty and Byrne (1999).

The pore-water pressure ratios of the nonliquefied soil elements in the upstream hydraulic fill (zone A in Fig. 12) are in the range of 5–25%. It is believed that the nonliquefied upstream zone with low pore-water pressures (zero pore-water pressure in the total stress model of Beaty and Byrne 1999) prevented the dam crest from moving downstream because of the little–nonreduced shear strength and stiffness. On the other hand, pore-water pressure ratios from the modified MFS model are in the range of 60–90% in the same nonliquefied zone. The much more softened nonliquefied upstream zone from the modified MFS model allows the dam crest to move more downstream. This mechanism clearly illustrates the importance of an effective stress analysis in a deformation analysis involving pore-water pressures.

## Conclusions

The following conclusions are drawn from the liquefaction and deformation analysis of the Upper San Fernando Dam using VERSAT (Wu 1998):

(1) Earthquake-induced deformation may be well predicted if the extent of liquefaction and amount of pore-water pressures can be predicted with confidence.

© 2001 NRC Canada

(2) The zone of liquefaction may be well assessed using the modified Martin–Finn–Seed pore-water pressure model proposed by Wu (1996). In using this model, the low-strain shear modulus can have a significant impact on the liquefaction assessment. The model tends to produce larger zones of liquefaction towards low modulus materials under the same level of shaking.

(3) An effective stress analysis including the effect of strain softening caused by excess pore-water pressures is necessary in earthquake deformation analysis involving pore-water pressures. Pore-water pressures in nonliquefied soil elements can have critical importance to the prediction of deformation magnitude.

(4) Cyclic resistance ratios, CRR, recommended by the NCEER (Youd and Idriss 1997) are representative when the shear stresses are calculated in a total stress approach. When they are applied in an effective stress analysis, the use of a low $\theta$ value in the Seed et al. (1976) pore-water pressure model is recommended to minimize the effect of pore-water pressures on the cyclic resistance. Alternatively, laboratory-measured cyclic resistance corresponding to an effective stress condition may be used.

(5) The hyperbolic nonlinear hysteretic stress–strain relationship can simulate well the stress–strain behavior of soil under cyclic loads. The application of the hyperbolic model should be used to the understanding of its limitation.

(6) The residual strengths of the liquefied hydraulic fill sands of the Upper San Fernando Dam were back-calculated from dynamic deformation analysis to be 23.0 kPa (480 psf) within the dam and 14.4 kPa (300 psf) in the downstream free field.

## References


Beaty, M., and Byrne, P. 1999. A simulation of the Upper San Fernando Dam using a synthesized approach. *In* Proceedings of the 13th Annual Vancouver Geotechnical Society Symposium, May, Vancouver, pp. 63–72.

Bhatia, S.K. 1980. The verification of relationships for effective stress method to evaluate liquefaction potential of saturated sands. Ph.D. thesis, Department of Civil Engineering, The University of British Columbia, Vancouver, B.C.

Byrne, P.M. 1991. A cyclic shear-volume coupling and pore pressure model for sand. *In* Proceedings of the 2nd International Conference on Recent Advances in Geotechnical Earthquake and Soil Dynamics, March, St. Louis, Mo., Vol. 1, pp. 47–56.

Byrne, P.M., Cheung, H., and Yan, L. 1987. Soil parameters for deformation analysis of sand masses. Canadian Geotechnical Journal, **24**: 366–376.

Finn, W.D.L. 1998. Seismic safety of embankment dams: developments in research and practice 1988–1998. *In* Proceedings of the 1998 Specialty Conference on Geotechnical Earthquake Engineering and Soil Dynamics III, Seattle. *Edited by* P. Dakoulas, M. Yegina, and B. Holtz. Geotechnical Special Publication 75, pp. 813–853.

Finn, W.D.L., Lee, K.W., and Martin, G.R. 1977. An effective stress model for liquefaction. Journal of the Geotechnical Engineering Division, ASCE, **103**: 517–533.

Finn, W.D.L., Yogendrakumar, M., Yoshida N., and Yoshida, H. 1986. TARA-3: a program for nonlinear static and dynamic effective stress analysis. Soil Dynamics Group, The University of British Columbia, Vancouver, B.C.

Finn, W.D.L., Sasaki, Y., Wu, G., and Thavaraj, T. 1999. Stability of flood protection dikes with potentially liquefiable foundations: analysis and screening criterion. *In* Proceedings of the 13th Annual Vancouver Geotechnical Society Symposium, May, Vancouver, B.C., pp. 47–54.

Gohl, B., Sorensen, E., Wu, G., and Pennells, E. 1997. Nonlinear soil–structure interaction analyses of a 2-span bridge on soft silt foundations. *In* Proceedings of the U.S. National Seismic Conference on Bridges and Highways, July, Sacramento, Calif., pp. 177–191.

Hardin, B.O., and Drnevich, V.P. 1972. Shear modulus and damping in soils: design equations and curves. Journal of the Soil Mechanics and Foundations Division, ASCE, **98**(7): 667–692.

Ishihara, K., and Yoshimine, M. 1992. Evaluation of settlements in sand deposits following liquefaction during earthquakes. Soils and Foundations, **32**(1): 173–188.

Itasca Consulting Group, Inc. 1998. FLAC – fast lagrangian analysis of continua. Version 3.40. Itasca Consulting Group, Inc., Minneapolis, Minn.

Martin, G.R., Finn, W.D.L., and Seed, H.B. 1975. Fundamentals of liquefaction under cyclic loading. Journal of the Geotechnical Engineering Division, ASCE, **101**(GT5): 423–438.

Moriwaki, Y., Tan, P., and Ji, F. 1998. Seismic deformation analysis of the Upper San Fernando Dam under the 1971 San Fernando earthquake. *In* Proceedings of the 1998 Specialty Conference on Geotechnical Earthquake Engineering and Soil Dynamics III, Seattle. Geotechnical Special Publication 75, pp. 854–865.

Muraleetharan, K.K., Mish, K.D., Yogachandran, C., and Arulanandan, K. 1988. DYSAC2: dynamic soil analysis code for 2-dimensional problems. Department of Civil Engineering, University of California, Davis, Calif.

Newmark, N.M. 1965. Effects of earthquake on dams and embankments. Géotechnique, **15**(2): 139–160.

Popescu, R., and Prevost, J.H. 1995. Comparison between VELACS numerical "Class A" predictions and centrifuge experimental soil test results. Soil Dynamics and Earthquake Engineering, **14**(2): 79–92.

Prevost, J.H. 1981. DYNAFLOW: a nonlinear transient finite element analysis program. Department of Civil Engineering, Princeton University, Princeton, N.J.

Schnabel, P.B., Lysmer, J., and Seed, H.B. 1972. SHAKE: a computer program for earthquake response analysis of horizontally layered sites. UCB/EERC-72/12, Earthquake Engineering Research Centre, University of California, Berkeley, Calif.

Seed, H.B., and Harder, L.F. 1990. SPT-based analysis of cyclic pore pressure generation and undrained residual strength. *In* Proceedings of the H. Bolton Seed Memorial Symposium, University of California, Berkeley. *Edited by* J.M. Duncan. BiTech Publishers, Vancouver, B.C., Vol. 2, pp. 351–376.

Seed, H.B., and Idriss, I.M. 1970. Soil moduli and damping factors for dynamic response analyses. UCB/ERRC-70/10, Earthquake Engineering Research Center, University of California, Berkeley, Calif.

Seed, H.B., and Idriss, I.M. 1982. Ground motions and soil liquefaction during earthquakes. EERI Monograph, Earthquake Engineering Research Institute, Berkeley, Calif.

Seed, H.B., Lee, K.L., Idriss, I.M., and Makdisi, F. 1973. Analysis of the slides in the San Fernando dams during the earthquake of Feb. 9, 1971. UCB/ERRC-73/02, Earthquake Engineering Research Center, University of California, Berkeley, Calif.

Seed, H.B., Idriss, I.M., Makdisi, F., and Banerjee, N. 1975. Representation of irregular stress time histories by equivalent uniform stress series in liquefaction analyses. UCB/EERC-75/29, Earth-


© 2001 NRC Canada

quake Engineering Research Center, University of California, Berkeley, Calif.

Seed, H.B., Martin, P.P., and Lysmer, J. 1976. Pore-water pressure changes during soil liquefaction. Journal of the Geotechnical Engineering Division, ASCE, **102**(GT4): 323–346.

Seed, H.B., Wong, R.T., Idriss, I.M., and Tokimatsu, K. 1986. Moduli and damping factors for dynamic analyses of cohesionless soils. Journal of the Geotechnical Engineering Division, ASCE, **112**(11): 1016–1032.

Serff, N., Seed, H.B., Makdisi, F.I., and Chang, C.Y. 1976. Earthquake induced deformation of earth dams. UCB/ERRC-76/04, Earthquake Engineering Research Center, University of California, Berkeley, Calif.

Sun, J.I., Golesorkhi, R., and Seed, H.B. 1988. Dynamic moduli and damping ratios for cohesive soils. UCB/ERRC-88/15, Earthquake Engineering Research Center, University of California, Berkeley, Calif.

Wu, G. 1996. Volume change and residual pore water pressure of saturated granular soils to blast loads. Natural Sciences and Engineering Research Council of Canada, Ottawa.

Wu, G. 1998. VERSAT: a computer program for static and dynamic 2-dimensional finite element analysis of continua, release 98. Wutec Geotechnical International, Vancouver, B.C.

Youd, T.L., and Idriss, I.M. (*Editors*). 1997. Proceedings of the NCEER Workshop on Evaluation of Liquefaction Resistance of Soils. Technical Report NCEER-97-0022.

Zienkiewicz, O.C., Chan, A.H.C., Pastor, M., Paul, D.K., and Shiomi, T. 1990*a*. Static and dynamic behaviour of soils: a rational approach to quantitative solutions. Part I: Fully saturated problems. Proceedings of the Royal Society of London, Series A, **429**: 285–309.

Zienkiewicz, O.C., Xie, Y.M., Schrefler, B.A., Ledesma, A., and Bicanic, N. 1990*b*. Static and dynamic behaviour of soils: a rational approach to quantitative solutions. Part II: Semi-saturated problems. Proceedings of the Royal Society of London, Series A, **429**: 311–321.

© 2001 NRC Canada